Physica B 405 (2010) 4763–4767

Contents lists available at ScienceDirect

Physica B

journal homepage: www.elsevier.com/locate/physb

Optical properties of silicon doped ZnO

R. Chowdhury *, S. Adhikari, P. Rees

Multidisciplinary Nanotechnology Centre, Swansea University, Swansea SA2 8PP, UK

ARTICLE INFO

Article history:
Received 28 July 2010
Received in revised form
26 August 2010
Accepted 30 August 2010

Keywords:
Wurtzite ZnO
First principles
Optical properties

ABSTRACT

We have calculated the optical structure of wurtzite ZnO doped with Silicon (Si). The calculations are based on the density functional theory with the generalized gradient approximation (GGA) and the projector augmented wave pseudopotentials. The GGA with the Perdew Burke Ernzerhof exchange-correlation functional are employed in the simulations. Ultrasoft pseudopotentials are utilized for the geometry optimization to render the computations tractable as well as to enhance the efficiency. We investigate two kinds of defects in ZnO, namely the substitution of Zn by Si and O by Si. The optical properties, including dielectric function, reflectivity and absorption coefficient of wurtzite ZnO are calculated. The variation in the band gap and energetics have been validated against published results. The dielectric properties follow a steep decreasing trend for the low energy level. In addition, the reflectivity and absorption coefficients reduce abruptly due to the doping.

© 2010 Elsevier B.V. All rights reserved.

1. Introduction

ZnO is a wide-gap semiconductor [1] and a promising material for electronic [2–6], piezoelectric [7] and optical [8–12] applications. With a band gap of $\sim$3.37 eV [13,14] and a large exciton binding energy ($\sim$60 meV) at the room temperature, ZnO [15] has many potential applications such as surface acoustic wave [16] devices, transparent conductive films, and gas detectors. More attention has been paid to thin films of ZnO, due to their potential applications in optoelectronic devices [17] in blue and ultraviolet spectra of light. ZnO has three well-known polymorphs: (i) wurtzite (P63/mc space group); (ii) zinc blende (F43m) and (iii) rocksalt (Fm/3m). Among them, wurtzite structure is more stable thermodynamically at ambient conditions. Due to the key role of Silicon (Si) in the modern semiconductor industry it is inevitable that researchers are very comfortable with working with Si for growing nanostructures. Additionally, Si is also a well known dopant that predominantly occupies cation sites in III–V semiconductors to improve their electrical and optical properties [18]. Therefore, using Si as a dopant material in ZnO might not only tune the electronic properties of ZnO, but also can enhance its usefulness in Si-related devices [19]. The similarity of Si and Zn atoms arises in terms of their electronegativity of 1.9 and 1.65 [20] and also their comparable atomic sizes of 0.117 and 0.133 nm [20], respectively. As a rule, Si tends to diffuse quickly into the ZnO lattice and forms a new phase Zn_2SiO_4, especially under high temperature [18].

In this paper, an *ab initio* calculation based on density functional theory (DFT) [21–24] is applied to investigate wurtzite ZnO and related Si-doped ZnO structures. We investigate two kinds of defects in ZnO, namely the substitution of Zn by Si and O by Si. The optical properties, including dielectric function, reflectivity and absorption coefficient of wurtzite ZnO are calculated. Throughout the text we used following notations: Substitutional Si on the Zn site is denoted as Si_{Zn}; substitutional Si on the O site is denoted as Si_O and substitutional Si on the both Zn and O site is denoted as Si_{ZnO}.

2. Computational approach

The ideal ZnO has a hexagonal wurtzite structure with the space group P63/mc and C6v-4 symmetry [25]. The cell parameters are $a=b = 3.249$ Å, $c = 5.206$ Å, $\alpha=\beta=90^{\circ}$, and $\gamma=120^{\circ}$ [25]. To illustrate the atom coordinates, a $2\times2\times2$ [6,13] supercell (with 28 atoms) of the wurtzite ZnO is shown in Fig. 1, which is frequently used in defect studies of ZnO. The O_{2-} coordination polyhedron is an O–Zn_4 tetrahedron, so it is a Zn_{2+} coordination polyhedron [6]. In order to address the finite size effect of the supercell, we performed the calculations considering 380 atoms (cell volume=96 times of primitive cell) in the supercell. The calculations are based on the density functional theory with the generalized gradient approximation (GGA) and the projector augmented wave pseudopotentials, as implemented in the CASTEP code [26,27]. CASTEP is based on a supercell approach, wherein all studies are performed on a periodic system. The main advantage of imposing the periodic boundary conditions relates to Bloch's theorem, which states that

* Corresponding author. Tel.: +44 1792 602088; fax: +44 1792 295676.
E-mail addresses: R.Chowdhury@swansea.ac.uk, crajib2003@gmail.com (R. Chowdhury).

0921-4526/$ - see front matter © 2010 Elsevier B.V. All rights reserved.
doi:10.1016/j.physb.2010.08.072

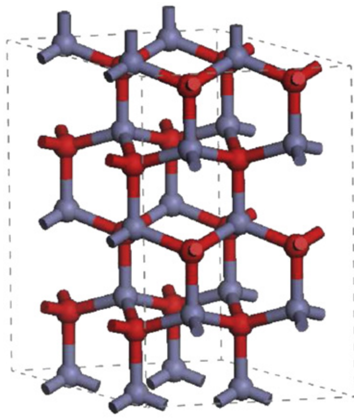

Fig. 1. Wurtzite ZnO with $2\times2\times2$ supercell. Atom colour in red corresponds to Oxygen atoms and others are Zinc atoms. (For interpretation of the references to color in this figure legend, the reader is referred to the web version of this article.)

in a periodic system each electronic wave function can be written as a product of a cell-periodic part and a wavelike part:

$$\psi_i(\mathbf{r}) = e^{i\mathbf{kR}}\psi_i(\mathbf{r}) \tag{1}$$

The cell periodic part, ψ, can then be expanded using a basis set consisting of a discrete set of plane waves whose wave vectors are reciprocal lattice vectors of the crystal:

$$\psi_i(\mathbf{r}) = \sum C_{i,\mathbf{G}}e^{i\mathbf{GR}} \tag{2}$$

Therefore, each electronic function can be written as a sum of plane waves, $\exp[i(\mathbf{k}+\mathbf{G})\bullet\mathbf{R}]$. Advantages and technical details of the plane wave basis set are described in a separate section. Among the major gains is the simplified form of the Kohn–Sham equations:

$$\sum[|\mathbf{k}+\mathbf{G}|^2\delta_{\mathbf{GG}'}+V_{ion}(\mathbf{G}-\mathbf{G}')+V_H(\mathbf{G}-\mathbf{G}')+V_C(\mathbf{G}-\mathbf{G}')]C_{i,\mathbf{k}+\mathbf{G}'} = \varepsilon_i C_{i,\mathbf{k}+\mathbf{G}'} \tag{3}$$

In this form, the kinetic energy is diagonal, and the various potentials are described in terms of their Fourier transforms. Another advantage of the plane wave basis set is the ease of calculating derivatives of the total energy with respect to atomic displacements, so that efficient geometry optimization can be done. However, there is an additional cost in using the supercell approach for systems that lack periodicity in three dimensions inherently. It is essential to introduce enough separation between the artificial images of such nonperiodic objects to ensure that there is no appreciable interaction between them.

The GGA with the Perdew Burke Ernzerhof exchange-correlation functional are employed in the simulations. Ultrasoft pseudopotentials [28] are utilized for the geometry optimization (Broyden–Fletcher–Goldfarb–Shanno algorithm) to render the computations tractable as well as to enhance efficiency. In addition, we performed calculation using screened exchange functional with LDA correlation (sX-LDA) [29]. sX-LDA is developed in the context of the generalized Kohn–Sham procedure [30], which allow to split the exchange contribution to the total energy into a screened, nonlocal and a local density component. However, this is exceedingly complex and extremely time consuming. Norm-conserving pseudopotentials are used with sX-LDA functional. In our calculation, a $4\times4\times4$ k-point Monkhorst–Pack mesh [31] in the Brillouin zone is used, the cutoff energy of the plane wave is 460 eV, and the calculation precision is set to be 2.0×10^{-5} eV/atom. All atoms were allowed to relax until the force on each atom was below 0.01 eV/Å and displacement of each atom was below 0.005 Å.

3. Results and discussion

3.1. Validation

The optimization of the supercell is the first step in the calculation. The optimized results of the primitive cell of pure ZnO are presented in Table 1. The optimized geometry parameters and formation energies are in good agreement with experimental results [25] and previous theoretical prediction. Our calculated ground state properties are tabulated in Table 2, which are in good agreement with other GGA and local density approximation (LDA) results [34–36]. Table 2 lists the calculated binding energies E_b, bulk modulus B_0 and band gap in different studies. We first calculate the electronic structure of the undoped ZnO crystal using GGA and sX-LDA functionals. Kohn–Sham schemes based on GGA functionals have a common feature: it underestimates the band gap substantially and in the present case it is about 0.73 eV. This is in good agreement with other calculations [6,32,38,39], but significantly smaller than the experimental value of 3.37 eV [25,37]. This does not affect the accuracy of the description of the total energy and related properties of crystals and molecules (equilibrium structure, vibrational spectra, elastic constants, etc.). However, an accurate description of the details of the electronic structure is often required to understand the properties of semiconductors and insulators. The DFT band gap error can be corrected either by using hybrid functional (sX-LDA functional used in this study) or introducing an empirical scissors correction. Using sX-LDA functional we found that band gap error is −0.59%, compared with the experiment. But this approach is extremely time consuming and it would be much suitable for crystal structure with primitive cell. For semiconductors, it is shown computationally (by comparing GW approximation and DFT band structures) that most of the difference between Kohn–Sham eigenvalues and the true excitation energies can be accounted for by a rigid shift of the conduction band upward with respect to the valence band [40]. This is attributed to a discontinuity in the exchange-correlation potential as the system goes from (N)-electrons to (N+1)-electrons during the excitation process. Using the same approach, named as scissor approximation (SA), we found that calculated the band gap becomes 3.37 eV, which is

Table 1
Comparison of the optimized results of the primitive cell of ZnO and the experimental data.

	a (Å)	c (Å)	c/a	V_0 (Å^3)	ΔH_f
Computed value (GGA functional)	3.2832	5.2983	1.6137	49.461	−3.06
Computed value (sX-LDA functional)	3.2493	5.2054	1.6020	47.595	−3.62
HSE approach [32]	3.2300	5.2500	1.6253	–	−3.66
Experimental value [6,25,33]	3.2501	5.2071	1.6021	48.335	−3.64

a and c are the lattice parameters. V_0 is the volume. ΔH_f is the formation enthalpy, which is defined as $\mu_{Zn}+\mu_O=\Delta H_f(ZnO)$. μ_{Zn} is the chemical potential of Zn; μ_O oxygen, referenced to the energy per atom of an isolated O_2.

Table 2
Comparison of the present work and other calculations and the experimental data.

	E_b (eV)	B_0 (GPa)	Band gap (eV)
Present work	7.46	138	0.73
GGA-PW91 [34]	7.35	136	0.91
GGA [35,36]	7.69	149	0.75
LDA [36]	9.769	162.3	0.79
Experiment [25,37]	7.56	142.6	3.37

E_b and B_0 denote binding energy and bulk modulus of ZnO crystal.

in excellent agreement with the experimental results as well with sX-LDA functional result. However, for the doped system only GGA functional is used to enhance computational efficiency. The variation in the electronic structure can result in different physical properties of the material, especially, the optical properties arising due to the electronic transitions. In the following section, different optical properties are presented.

3.2. Optical properties

The optical properties of a material can be described by means of the dielectric function $\varepsilon(\omega)$. It primarily relates to the electronic response. The imaginary part $\varepsilon_2(\omega)$ of dielectric function is calculated using the following expression:

$$\varepsilon_2 = \frac{2e^2\pi}{\Omega\varepsilon_0}\sum_{\mathbf{k},\upsilon,\mathbf{c}} |\langle \psi_{\mathbf{k}}^c | \mathbf{u}\cdot\mathbf{r} | \psi_{\mathbf{k}}^\upsilon \rangle|^2 \delta(\omega_{\mathbf{k}}^c - \omega_{\mathbf{k}}^\upsilon - \omega) \tag{4}$$

where $\mathbf{u}$ is the vector defining the polarization of the incident electric field. This expression is effectively Fermi's Golden rule for time dependent perturbations, and $\varepsilon_2(\omega)$ can be thought of as detailing the real transitions between occupied and unoccupied electronic states. Since the dielectric constant describes a causal response, the real and imaginary parts are linked by the Kramers–Kronig transform. This transform is used to obtain the real part of the dielectric function, $\varepsilon_1(\omega)$. The matrix elements of the position operator that are required to describe the electronic transitions in Eq. (4) may normally be written as matrix elements of the momentum operator allowing straightforward calculation in reciprocal space. However, this depends on the use of local potentials, while in CASTEP nonlocal potentials are more often used. The corrected form of the matrix elements is given by

$$\langle \psi_{\mathbf{k}}^c | \mathbf{r} | \psi_{\mathbf{k}}^\upsilon \rangle = \frac{1}{i\omega m}\langle \psi_{\mathbf{k}}^c | \mathbf{P} | \psi_{\mathbf{k}}^\upsilon \rangle + \frac{1}{\hbar\omega}\langle \psi_{\mathbf{k}}^c (|V_{nl}|,\mathbf{r}) \psi_{\mathbf{k}}^\upsilon \rangle \tag{5}$$

Ultrasoft pseudopotentials produce an additional contribution to the optical matrix elements which is included in present results. The intraband contribution to the optical properties affects mainly the low energy infra-red part of the spectra. It can be described sufficiently accurately via an semiempirical Drude term in the optical conductivity as

$$\varepsilon_D(\omega) = 1 - \frac{\omega_P^2}{\omega(i\gamma_D + \omega)} \tag{6}$$

Here the plasma frequency ω_P and the damping parameter γ_D depend on several details of the material and is usually obtained from the experiment. The Drude damping parameter describes the broadening of the spectra due to effects not included in the calculation. Examples of processes that contribute to this broadening are electron–electron scattering (including Auger processes), electron–phonon scattering, and electron-defect scattering. This last contribution is usually the most important.

The level of approximation used here does not take any local field effects into account. These arise from the fact that the electric field experienced at a particular site in the system is screened by the polarizability of the system itself. So, the local field is different from the applied external field (that is, the photon electric field). This can have a significant effect on the spectra calculated but it is prohibitively expensive to calculate for general systems. In connection with the absence of local field effects, excitonic effects are not treated in the present study. The nonlocal nature of the GGA functionals is not taken into account when evaluating the matrix elements but it is expected that this will have a small effect on the calculated spectra. Phonons and their optical effects have been neglected.

All the other optical constants, such as refractive index $n(\omega)$, absorption coefficient $a(\omega)$, reflectivity $R(\omega)$, and energy-loss spectrum $L(\omega)$ can be derived from $\varepsilon_1(\omega)$ and $\varepsilon_2(\omega)$ as follows:

$$n(\omega) = \sqrt{\varepsilon_1(\omega) + i\varepsilon_2(\omega)} \tag{7}$$

$$a(\omega) = \frac{2k\omega}{c} \tag{8}$$

$$R(\omega) = \left|\frac{1-n(\omega)}{1+n(\omega)}\right|^2 \quad \text{and} \tag{9}$$

$$L(\omega) = \mathrm{Im}\left(-\frac{1}{\varepsilon_1(\omega) + i\varepsilon_2(\omega)}\right) \tag{10}$$

Fig. 2 shows the dielectric functions of ZnO at ambient conditions. Since the crystal has similar dielectric response in the cases of the electric field parallel to and normal to the c-axis [9], polycrystalline case (no direction is specified, the electric field vectors are taken as a fully isotropic average) is considered for evaluating the optical properties. The results for the dispersive part of the dielectric function $\varepsilon_1(\omega)$ of the ZnO is presented in Fig. 2(a), which agrees well with the previous results [3,9] and experiment [41]. The main features for undoped ZnO crystal are: (i) a peak at around 3 eV; (ii) another two lower peaks located at about 7 and 11 eV, inside of which $\varepsilon_1(\omega)$ decreased toward zero then becomes negative finally reached a minimum; and then again a slight increase toward zero at higher energies. For Si_{Zn} system, there is steep decrease in $\varepsilon_1(\omega)$ between 0 and 2 eV, which goes toward zero then becomes negative finally reached a minimum. For Si_O system, almost steady steep decrease in $\varepsilon_1(\omega)$ is observed. Similarly, For Si_{ZnO} system, almost steady steep decrease in $\varepsilon_1(\omega)$ is observed, except a peak at around 2 eV. The absorptive part of the dielectric function $\varepsilon_2(\omega)$ of the ZnO polycrystalline is presented in Fig. 2(b). The starting point of the optical response is nearly 0 eV. According to the electric transition theory of dielectric response, the low-energy edge of $\varepsilon_2(\omega)$ is related to the selection rules of electric transition in optical one-photon process. It is known that the photon–electron coupling may lead to the transition between occupied and unoccupied states and therefore the starting point of the native optical response should be at least larger than the band gap. Zero starting point implies the existence of some other transition style nearby but left to the native absorption the intra-band transitions of the thermal electrons. It is found that, dielectric function of ZnO can be divided into two spectral regions, namely, the low-energy region and the high-energy region. In the present study, for dielectric functions of $\varepsilon_2(\omega)$ in the energy range of 1–11 eV, the peak at about 6 eV is assigned to the transition from the highest valence band to the lowest conduction band. For Si_{Zn} system, there is steep increase in $\varepsilon_2(\omega)$ and the highest peak is found at about 1.5 eV, compared to undoped system. The peaks at about 5.5 and 9.6 eV may be related to transitions between valence band and higher conduction bands. For Si_O system, the peak occurs at about 4 eV. It is found that, the peaks are shifted to the lower energy region, compared with undoped system. The shift of the peaks can be attributed to the variation of band structure and to the transition between O 2p and the unoccupied Zn 5s. Similar variation can be observed in the reflectivity $R(\omega)$ and absorption coefficient $a(\omega)$, as shown in Fig. 3. The peak, in the energy scope of 5–15 eV, of the absorption coefficient $a(\omega)$ decreases from undoped to Si_{ZnO}, although same peak is observed for Si_{Zn}.

The loss function curves or energy-loss spectrum $L(\omega)$ are primarily used to describe the energy loss of a fast electron traversing in the material and its peaks are associated with the plasma frequency. All of the loss function curves present remarkable peaks in the energy scope of 12–18 eV, presented in Fig. 4. The positions of the peaks in $L(\omega)$ spectra correspond to the

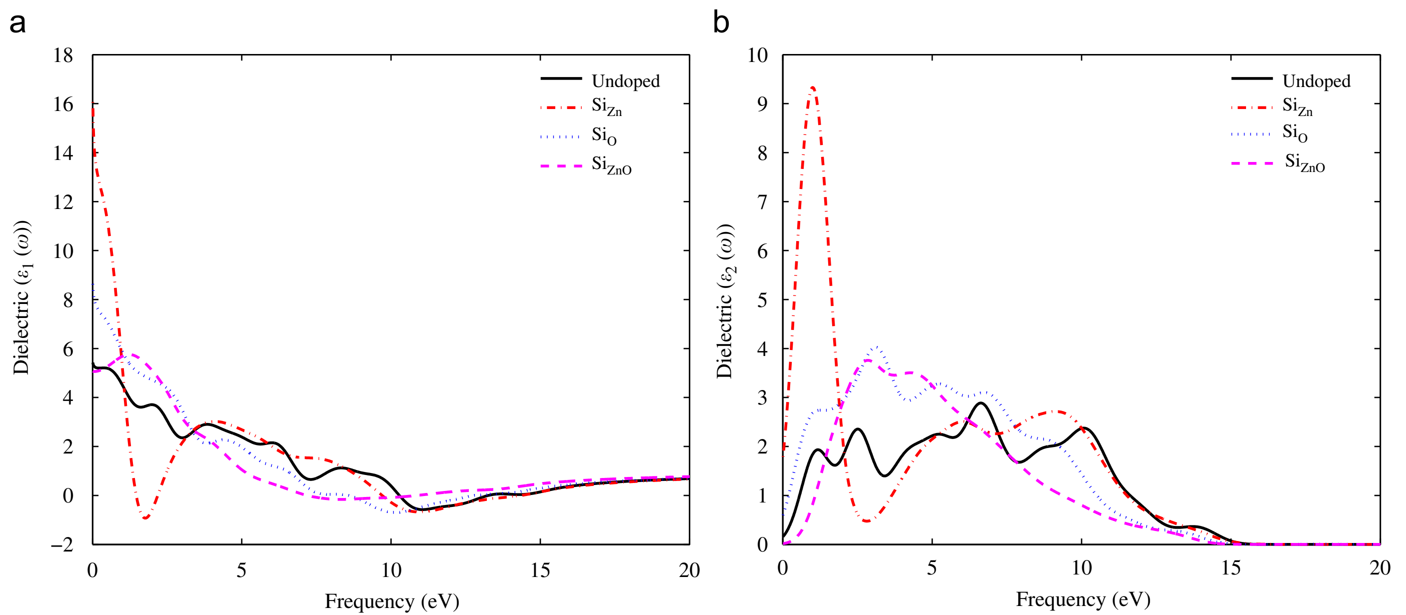

Fig. 2. The dielectric function of the ZnO crystal and the corresponding Si doped ZnO systems. For undoped ZnO crystal, a peak at around 3 eV and another two lower peaks located at about 7 and 11 eV is observed. $\varepsilon_1(\omega)$ decreased toward zero then becomes negative and finally reached a minimum. For the Si_{Zn} system, there is a steep decrease in $\varepsilon_1(\omega)$ between 0 and 2 eV, which goes toward zero then becomes negative and finally reached a minimum. For the Si_O system, almost steady steep decrease in $\varepsilon_1(\omega)$ is observed. Similarly, for the Si_{ZnO} system, almost steady steep decrease in $\varepsilon_1(\omega)$ is observed, except a peak at around 2 eV. The starting point of the optical response is nearly 0 eV. According to the electric transition theory of dielectric response, the low-energy edge of $\varepsilon_2(\omega)$ is related to the selection rules of electric transition in optical one-photon process. It is known that the photon–electron coupling may lead to the transition between occupied and unoccupied states and therefore the starting point of the native optical response should be at least larger than the band gap. Zero starting point implies the existence of some other transition style nearby but left to the native absorption the intra-band transitions of the thermal electrons. (a) Real part of the dielectric function $\varepsilon_1(\omega)$ of ZnO and (b) imaginary part of the dielectric function $\varepsilon_2(\omega)$ of ZnO.

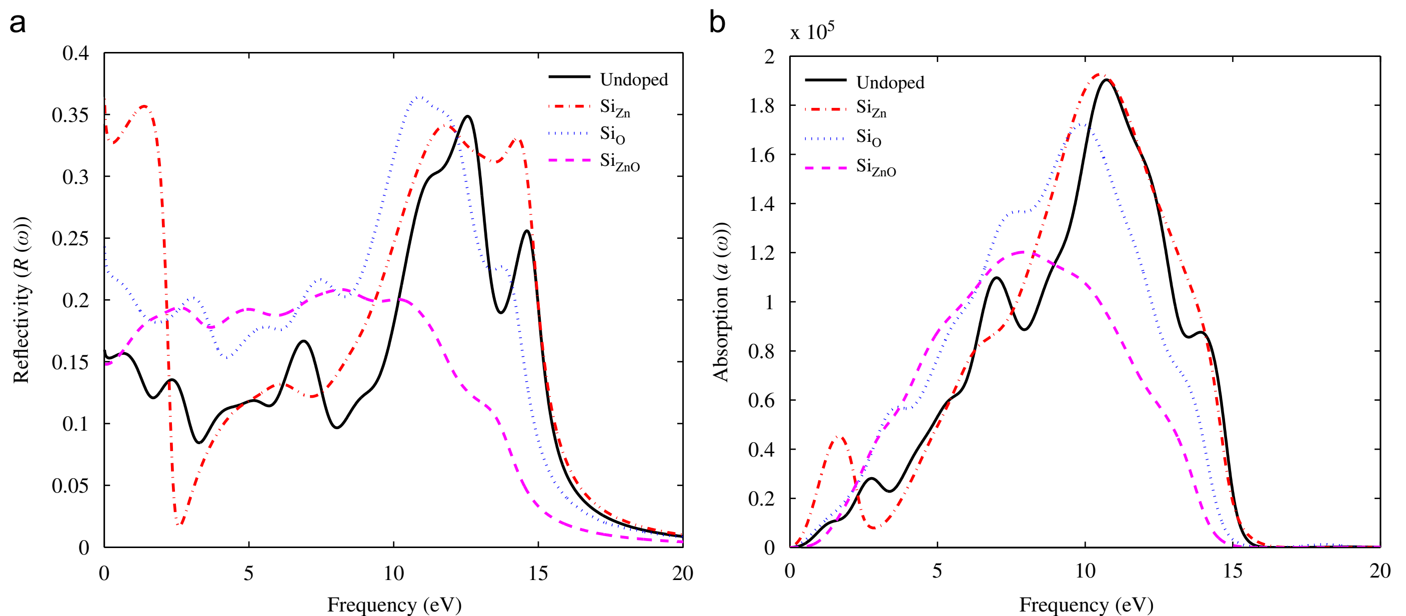

Fig. 3. Reflectivity and absorption coefficient of the ZnO crystal and the corresponding Si doped ZnO systems. The peaks occur in the energy scope of 5–15 eV. However, there is substantial decrease in the peaks of the absorption for doped system. (a) Reflectivity $R(\omega)$ of ZnO and (b) absorption coefficient $a(\omega)$ of ZnO.

transformation from negative $\varepsilon_1(\omega)$ to positive $\varepsilon_1(\omega)$, indicating the transition from the metallic property to the dielectric property. For undoped ZnO, there is a single strong peak at around 14.5 eV. This is in agreement with the features of both $\varepsilon_1(\omega)$ curves, in which only one metallic region exists wurtzite ZnO; while for Si_{Zn} system, there is a weak peak near at 2 eV and a strong peak at 13 eV. Furthermore, it can be observed that, Si_{ZnO} the peak is reduced to 2.2 units from 4.2 units for undoped case. In addition, corresponding to the energy position of peaks in $L(\omega)$, the reflectivity and absorption coefficients reduce abruptly (ref. Fig. 3).

4. Conclusion

We have performed first-principles calculations of Si-doped ZnO systems with Si at different sites. The calculations are based on the density functional theory with the generalized gradient

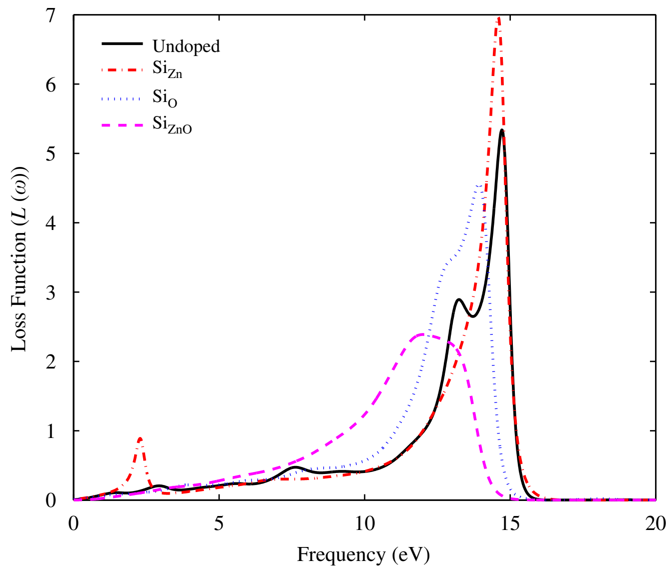

Fig. 4. The loss function of the ZnO crystal and the corresponding Si doped ZnO systems. The loss function curves are primarily used to describe the energy loss of a fast electron traversing in the material and its peaks are associated with the plasma frequency. All of the loss function curves present remarkable peaks in the energy scope of 12–18 eV.

approximation and the projector augmented wave pseudopotentials. The main dielectric features for Si doped ZnO are: for Si_{Zn} system, there is a steep decrease in $\varepsilon_1(\omega)$ between 0 and 2 eV. For Si_O system, almost steady steep decrease in $\varepsilon_1(\omega)$ is observed. Similar observation can also be made for Si_{ZnO} system, except a peak at around 2 eV. The peak at about 6 eV of $\varepsilon_2(\omega)$ corresponds to the transition from the highest valence band to the lowest conduction band. For undoped ZnO, there is a single strong peak at around 14.5 eV in the energy-loss spectrum. This is in agreement with the features of both $\varepsilon_1(\omega)$ curves, in which only one metallic region exists wurtzite ZnO; while for Si_{Zn} system, there is a weak peak near 2 eV and a strong peak at 13 eV. In addition, corresponding to the energy position of peaks in $L(\omega)$, the reflectivity and absorption coefficients reduce abruptly.

Acknowledgements

RC acknowledges the support of Royal Society through the award of Newton International Fellowship. SA gratefully acknowledges the support The Leverhulme Trust for the award of the Philip Leverhulme Prize.

References

[1] U. Ozgur, Y. Alivov, C. Liu, A. Teke, M. Reshchikov, S. Dogan, V. Avrutin, S. Cho, H. Morkoc, Journal of Applied Physics 98 (2005).
[2] X.D. Zhang, M.L. Guo, C.L. Liu, L.A. Zhang, W.Y. Zhang, Y.Q. Ding, Q. Wu, X. Feng, European Physical Journal B 62 (2008) 417.
[3] X.B. Chen, L. Qi, M.Z. Ma, Q. Jing, G. Li, W.K. Wang, R.P. Liu, Solid State Communications 145 (2008) 267.
[4] Y.Q. Gai, B. Yao, Y.M. Lu, D.Z. Shen, J.Y. Zhang, D.X. Zhao, X.W. Fan, Physics Letters A 372 (2007) 72.
[5] Q. Yu, W. Fu, C. Yu, H. Yang, R. Wei, Y. Sui, S. Liu, Z. Liu, M. Li, G. Wang, et al., Journal of Physics D—Applied Physics 40 (2007) 5592.
[6] S. Panpan, S. Xiyu, H. Qinying, L. Yadong, C. Wei, Journal of Semiconductors 30 (2009).
[7] R. Chowdhury, S. Adhikari, F. Scarpa, Physica E—Low-Dimensional Systems & Nanostructures 42 (2010) 2036.
[8] J. Sans, A. Segura, F. Manjon, B. Mari, A. Munoz, M. Herrera-Cabrera, Microelectronics Journal 36 (2005) 928.
[9] X. Tang, H.F. Lu, C.Y. Ma, J.J. Zhao, Q.Y. Zhang, Physics Letters A 372 (2008) 5372.
[10] Z. Fu-Chun, Z. Zhi-Yong, Z. Wei-Hu, Y. Jun-Feng, Y. Jiang-Ni, Chinese Physics Letters 25 (2008) 3735.
[11] Y.-I. Kim, R. Seshadri, Inorganic Chemistry 47 (2008) 8437.
[12] Y. Yu, J. Zhou, H. Han, C. Zhang, T. Cai, C. Song, T. Gao, Journal of Alloys and Compounds 471 (2009) 492.
[13] Q. Wan, Z. Xiong, J. Dai, J. Rao, F. Jiang, Optical Materials 30 (2008) 817.
[14] Y. Yu-Rong, Y. Xiao-Hong, G. Zhao-Hui, D. Yu-Xiang, Chinese Physics B 17 (2008) 3433.
[15] F. Decremps, F. Datchi, A. Saitta, A. Polian, S. Pascarelli, A. Di Cicco, J. Itie, F. Baudelet, Physical Review B 68 (2003).
[16] R. Chowdhury, S. Adhikari, F. Scarpa, Applied Physics A: Materials Science & Processing, in press, doi:10.1007/s00339-010-5995-3.
[17] D. Look, B. Claftin, Physica Status Solidi B—Basic Research 241 (2004) 624.
[18] J. Zhao, L. Qin, L. Zhang, Physica E—Low-Dimensional Systems & Nanostructures 40 (2008) 795.
[19] R. Chowdhury, P. Rees, S. Adhikari, F. Scarpa, S.P. Wilks, Physica B—Condensed Matter 405 (2010) 1980.
[20] X. An, G. Meng, Q. Wei, L. Zhang, Crystal Growth & Design 6 (2006) 1967.
[21] N.H. Moreira, G. Dolgonos, B. Aradi, A.L. da Rosa, T. Frauenheim, Journal of Chemical Theory and Computation 5 (2009) 605.
[22] B. Wang, S. Nagase, J. Zhao, G. Wang, Nanotechnology 18 (2007).
[23] Y.R. Yang, X.H. Yan, Y. Xiao, Z.H. Guo, Chemical Physics Letters 446 (2007) 98.
[24] N.H. Moreira, A.L. da Rosa, T. Frauenheim, Applied Physics Letters 94 (2009).
[25] E. Kisi, M. Elcombe, Acta Crystallographica Section C—Crystal Structure Communications 45 (1989) 1867.
[26] S. Clark, M. Segall, C. Pickard, P. Hasnip, M. Probert, K. Refson, M. Payne, Zeitschrift Fur Kristallographie 220 (2005) 567.
[27] M. Segall, P. Lindan, M. Probert, C. Pickard, P. Hasnip, S. Clark, M. Payne, Journal of Physics-Condensed Matter 14 (2002) 2717.
[28] D. Vanderbilt, Physical Review B 41 (1990).
[29] J. Lento, R. Nieminen, Journal of Physics-Condensed Matter 15 (2003) 4387.
[30] A. Seidl, A. Gorling, P. Vogl, J. Majewski, M. Levy, Physical Review B 53 (1996) 3764.
[31] H. Monkhorst, J. Pack, Physical Review B 13 (1976) 5188.
[32] J.L. Lyons, A. Janotti, C.G. Van de Walle, Physical Review B 80 (2009).
[33] A. Janotti, D. Segev, C.G. Van de Walle, Physical Review B 74 (2006).
[34] Z. Fu-Chun, Z. Zhi-Yong, Z. Wei-Hu, Y. Jun-Feng, Y. Jiang-Ni, Chinese Physics B 18 (2009) 2508.
[35] P. Erhart, K. Albe, A. Klein, Physical Review B 73 (2006).
[36] J. Jaffe, J. Snyder, Z. Lin, A. Hess, Physical Review B 62 (2000) 1660.
[37] S. Desgreniers, Physical Review B 58 (1998) 14102.
[38] D. Vogel, P. Kruger, J. Pollmann, Physical Review B 52 (1995) 14316.
[39] Y. Xu, W. Ching, Physical Review B 48 (1993) 4335.
[40] R.W. Godby, Topics in Applied Physics 69 (1992).
[41] J.L. Freeouf, Physical Review B 7 (1973) 3810.